Choosing the Right Signal: Doppler Shift Estimation for Underwater Acoustic Signals*

Roee Diamant
Department of Electrical and Computer Engineering
The University of British Columbia (Canada)
roeed@ece.ubc.ca

Arie Feuer
Department of Electrical Engineering
The Technion (Israel)
feuer@ee.technion.ac.il

Lutz Lampe
Department of Electrical and Computer Engineering
The University of British Columbia (Canada)
roeed@ece.ubc.ca

ABSTRACT

In this paper, we consider the problem of estimating the coarse Doppler shift ratio for underwater acoustic communication (UWAC). Since underwater the constant motion of nodes results in Doppler shifts that significantly distort received signals, estimating the Doppler shift and compensating for it is required for all UWAC applications. Different than for terrestrial radio-frequency where the Doppler effect is modeled by a frequency shift, due to the slow sound speed in water, the effect of transceiver motion on the duration of the symbol cannot be neglected. Furthermore, since the carrier frequency and the signal bandwidth are of the same order, UWAC signals are considered wideband and Doppler-induced frequency shifts cannot be assumed fixed throughout the signal bandwidth. Considering these challenges, we present a method for Doppler-shift estimation based on comparing the arrival times of two chirp signals and approximating the relation between this time difference and the Doppler shift ratio. This analysis also provides an interesting insight about the resilience of chirp signals to Doppler shift. Our simulation results demonstrate improvement compared to commonly used benchmark methods in terms of accuracy of the Doppler shift estimation at near-Nyquist baseband sampling rates.

Keywords

Doppler Shift, Underwater Acoustic Communication, LFM chirp, QFM chirp

1. INTRODUCTION

Underwater acoustic communication (UWAC) has a large variety of applications. A brief list of examples includes oceanography data collection, ocean exploration, undersea navigation and control over autonomous underwater vehicles [2]. While current research involves all layers of UWAC networks, the basic demands remains to ensure a certain reliability in decoding the transmitted communication symbols. Reliable UWAC is challenging due to the characteristics of the underwater acoustic channel. These include a high power attenuation, small bandwidth, fast time-varying impulse response, and considerable Doppler shift [1]. Recently, there have been significant efforts to design robust receivers which successfully equalize the channel, and achieved transmission rates have significantly increased [5].

Among the unique characteristics of the UWAC channel is the Doppler shift. Unlike the case of radio frequency communication for which the Doppler shift is usually modeled as a frequency offset and the effect of Doppler shift (or transceiver motion) on the symbol duration is neglected, in UWAC the later assumption cannot be made. We refer to the latter phenomenon as *Doppler scaling*. While vessels usually move slowly in water, the low sound speed (roughly 1500 m/sec) results in possibly large Doppler shift ratios, and due to the low transmission rate, Doppler scaling may significantly extend or shorten the duration of the received communication symbols. Since, underwater nodes can move in all directions and even a seemingly static node moves around its anchor, Doppler shift estimation and compensation are required for any UWAC application.

In this paper, we consider the problem of providing a coarse estimate of the Doppler shift, which is the average value over the Doppler shifts of different signal paths. In the UWAC literature, Doppler shift estimation has been extensively explored. Most proposed methods rely on a synchronization signal with good resilience to Doppler shift, and estimate the coarse Doppler shift by either passing the received symbol through a bank of matched filters (MF), each matched to a different tested Doppler shift ratio, or measuring the received symbol frequency offset or the change to the symbol duration. The latter is performed by measuring the time-difference-of-arrival (TDoA) between two received symbols and comparing it to the expected value. Then, the information bearing symbols are interpolated at the estimated coarse Doppler shift ratio and a fine Doppler shift estimation and tracking is performed, usually using a phase locked loop [12]. However, a bank of MF highly increases complexity, and direct measurement of the symbol extension or the frequency offset requires fine sampling resolution, which sets limits on the baseband sampling frequency being

*This work was supported by the National Sciences and Engineering Research Council (NSERC) of Canada through a Vanier Scholarship and a Strategic Project Grant.

used and, again, increases complexity. Moreover, to the best of our knowledge, there has not been a thorough study on the optimal structure of the synchronization signal.

Considering the problem of fine sampling resolution required for Doppler shift estimation using the existing methods, we suggest a new method to effectively estimate the coarse Doppler shift for underwater acoustic communication. Our method involves measuring the TDoA between increasing frequency (*Up*) and decreasing frequency (*Down*) received chirp symbols. We refer to the suggest method as the *Up-Down* Doppler shift estimation method. We do not directly measure the change to the symbol duration. Instead, we propose a method to measure the time offset, caused by Doppler shift, for the arrival of the symbol. By calculating the relationship between this measured time offset and the Doppler shift ratio, we are able to estimate the latter. This method allows us to simultaneously transmit the Up and Down chirps, thus increasing throughput compared to sending two separate symbols in TDoA Doppler shift estimation method. Furthermore, we prove that the minimum sampling frequency needed to estimate Doppler shift at a certain resolution is lower than that for directly measuring the Doppler scaling. While a similar method has been suggested for radar detection (e.g., [10]), our contribution lies in adapting it to UWAC and deriving an approximation for the above relationship considering also the effect of Doppler scaling. We perform this (non-trivial) analysis for two types of exponential chirp signals, namely the linear-frequency-modulation (LFM) and the quadratic-frequency-modulation (QFM), where the former is extensively used in radar detection [10], and conclude that the QFM chirp is more resilient to Doppler shifts. Similar analysis can be made for other types of chirp signals, for example the hyperbolic-frequency-modulation (HFM) which is also used for underwater acoustic target tracking [15]. We present simulation results showing that in near-Nyquist baseband sampling rates, our method provides a more accurate coarse Doppler shift estimation than widely used benchmark methods.

The remainder of this paper is organized as follows. Related work is discussed in Section 2. System model and objectives are introduced in Section 3. In Section 4.1 we give an intuition to our approach, in Section 4.2 we describe the details of our method, and LFM and QFM signals are compared in Section 4.3. Simulation results are presented in Section 5, and conclusions are offered in Section 6.

2. RELATED WORK

In UWAC, synchronization signals are used for detection purposes, coarse channel estimation, and time synchronization [17]. Usually, detection is performed using an MF. Thus, the effect of Doppler shift on the output of the MF should be as small as possible. Moreover, to allow multipath separation, the auto-correlation of the synchronization signal should be as narrow as possible, i.e. a wideband signal is required. Most works consider the use of chirp signals for the synchronization signal (e.g., [17, 11, 18, 6]). The chirp signal is widely used in radar [10] and sonar applications [15]. It is resilient to Doppler shift, and has a low peak-to-average ratio. The latter characteristic makes the chirp signal suitable for transmission using switching power amplifiers, which are commonly used in UWAC due to their high efficiency.

We identify four main approaches for coarse Doppler estimation. The first includes a bank of M MFs, each branch corresponds to a different Doppler shift ratio [11, 14]. The received symbol is passed through the MFs, and the Doppler shift ratio is estimated according to the branch that produces the highest energy at the matching point. The accuracy of this method depends on the resolution of the tested Doppler shift ratios, i.e., the number M. However, increasing M also increases the complexity, and the latter is especially important since the synchronization signal should be detected in real-time.

A second approach to estimate the coarse Doppler shift relies on measuring the Doppler-induced frequency offset. The received synchronization signal is converted to the frequency domain and a detector is used to estimate the received carrier frequency. Then, the Doppler shift ratio is obtained as a function of the frequency offset and the estimated propagation speed [12]. This (rather straight-forward) approach is hardly in use since 1) most synchronization signals in use are wideband signals, 2) carrier frequency estimation requires high signal-to-noise ratio (SNR), and 3) detection at the frequency domain sets hard limitations on the baseband sampling frequency in use, which increases complexity.

A different approach considers the coarse Doppler shift as part of the channel parameters. In [9], the received signal is decomposed into basis functions whose parameters fit the channel multipath, phase change, and Doppler shift. By optimizing the choice of these basis functions, the Doppler shift is estimated. An alternative approach by the same group is presented in [8], where channel parameters are estimated using the Merlin transform coefficients, which also include the Doppler shift ratio. Since the UWAC channel is highly complex, a model must be used to limit the number of estimated parameters. Thus, while this approach is more general, it is sensitive to channel model mismatch.

The most commonly used approach for Doppler shift estimation involves direct measuring of the Doppler scaling. In [12], this is performed by transmitting chirp signals from an array of transmitters and comparing the TDoA to the expected delay. In [18] and [16], a similar approach is taken by transmitting a pre-ample signal before the information packet and a post-ample signal after the information packet. The TDoA between the pre-ample and post-ample signals is compared to the duration of the transmitted packet to infer the Doppler shift ratio. When the duration of the information packet is large (and thus Doppler scaling is more noticeable), this method has the benefit of high accuracy. However, since the method assumes that the Doppler shift ratio is fixed between the pre-ample and post-ample symbols, this accuracy tradeoffs with the coherence time of the Doppler shift. In this paper we will also show that the above method also limits the sampling resolution, and at near-Nyquist baseband sampling frequencies accuracy is significantly affected.

3. SYSTEM MODEL

Our Doppler estimation method relies on a synchronization signal, which is transmitted as part of any packet. We assume that the receiver is aware of the structure of the synchronization signal but has no prior information of the relative velocity between the transmitter and receiver. The noise level and signal power attenuation in the channel are

assumed to permit reliable signal detection. Using the synchronization signal, our objective is to estimate the coarse Doppler shift.

3.1 Doppler Shift Model

When the receiver and transmitter move with relative speed v along the direction of the transmitted signal, Doppler shift occurs. The Doppler shift ratio is defined as $\mu = \frac{v}{c}$, where c is the propagation speed. Given Doppler shift ratio μ, a symbol $s(t)$ of duration T_s is received as [3]

$$\tilde{s}(t) = \underbrace{s(t(1+\mu)-\tau)}_{\tilde{s}_1} \cdot \underbrace{e^{-j\mu\omega_c t}}_{\tilde{s}_2}, \qquad 0 \le t \le T_s \ , \qquad (1)$$

where τ is the propagation delay, and ω_c is the angular carrier frequency of the transmitted signal. Terms $\tilde{s}_1$ and $\tilde{s}_2$ in (1) correspond to the time scaling of the received signal and a frequency offset, respectively. For a sampled signal $s[n]$, the Doppler shift phenomenon can be modeled by interpolating $s[n]$ at rate $1-\mu$.

3.2 Example for Doppler Shift Distortion

In the following we give an example to emphasize the need for accurate Doppler shift estimation and correction at the receiver. We measure the distortion, caused by the Doppler shift phenomenon, of the received symbol by the difference between the energy at the matching point of the matched filter (MF) output for a symbol with and without Doppler shift. For a transmitted symbol $s(t)$ and a received symbol $\tilde{s}(t)$, the MF output is given as

$$R(\tau) = \frac{1}{T_s}\int_0^{T_s} s(t)\tilde{s}(t-\tau)dt \ . \qquad (2)$$

To demonstrate the effect of Doppler shift, we consider the widely used direct-sequence-spread-spectrum (DSSS) signal. Let $a_n,\ n = 1,\ldots,N$ be a pseudo-random sequence such that

$$a = \begin{cases} +1 & \text{With Probability 0.5} \\ -1 & \text{With Probability 0.5} \end{cases} .$$

Also let L_c be the number of chips, each of duration $T_{\text{chip}} = \frac{T_s}{L_c}$. The baseband DSSS signal is given by [13]

$$s(t) = \sum_{n=0}^{L_c-1} a_n \cdot g(t - nT_{\text{chip}}) \ , \ 0 < t \le T_s \ , \qquad (3)$$

where, for simplicity, $g(t - T_{\text{chip}}) = u(t) - u(t - T_{\text{chip}})$, and $u(t)$ is the unit-step function. Given model (1), a DSSS signal (3) distorted by Doppler shift of ratio μ is expressed by

$$\tilde{s}(t) = \sum_{n=0}^{L_c-1} a_n \tilde{g}(t - n\tilde{T}_{\text{chip}}) \ , \ 0 < t \le \tilde{T}_{\text{chip}} L_c \ , \qquad (4)$$

where $\tilde{g}(t)$ is a rectangular pulse whose duration is $\tilde{T}_{\text{chip}} = \frac{T_{\text{chip}}}{1-\mu}$. The MF output (2) for a Doppler-induced DSSS signal is given by

$$\begin{aligned} R(\tau) &= \frac{1}{T_s}\int_0^{T_s} \sum_{m,n=0}^{L_c-1} a_n a_m g\left(t - nT_{\text{chip}}\right) \\ &\cdot \ \tilde{g}\left(t - m\tilde{T}_{\text{chip}} - \tau\right) dt \ . \end{aligned} \qquad (5)$$

Recall $E(a_n) = 0$. Thus, for a large number of chips (say $L_c > 12$), we are interested in the Doppler shift effect on $R(\tau)$ within a window of T_{chip} sec around the matching point (defined as $\tau = 0$). Here,

$$\begin{aligned} R(0) &= \frac{1}{T_s}\int_0^{T_s} \sum_{n=0}^{L_c-1} g\left(t - nT_{\text{chip}}\right) \\ &\cdot \ \frac{(n+1)\left(\tilde{T}_{\text{chip}} - T_{\text{chip}}\right)}{\tilde{T}_{\text{chip}}} dt \\ &+ \ \frac{1}{T_s}\int_0^{T_s} \sum_{n=0}^{L_c-1} g\left(t - nT_{\text{chip}}\right) \\ &\cdot \ \left(1 - \frac{(n+1)\left(\tilde{T}_{\text{chip}} - T_{\text{chip}}\right)}{\tilde{T}_{\text{chip}}}\right) dt \ . \end{aligned} \qquad (6)$$

Assuming $(L_c - 1)\left(\tilde{T}_{\text{chip}} - T_{\text{chip}}\right) \le T_{\text{chip}}$, the first term of (6) can be neglected. Thus,

$$\begin{aligned} R(0) &\approx \frac{1}{T_s} \cdot \frac{T_{\text{chip}}}{\tilde{T}_{\text{chip}}} \sum_{n=0}^{L_c-1} n\left(T_{\text{chip}} - \tilde{T}_{\text{chip}}\right) + T_{\text{chip}} \\ &= \frac{1}{1+\mu} - \frac{\mu(L_c-1)}{2} \ . \end{aligned} \qquad (7)$$

For $\mu = 0$, i.e., zero Doppler shift, the expression in (7) yields $R(0) = 1$. However, for $L_c = 100$ and as little as $\mu = 0.003$, i.e., relative speed of 4.5 m/sec and $c = 1500$ m/sec, we get $R(0) = 0.84$. That is, the Doppler shift results in 16% energy reduction at the MF output.

3.3 The Chirp Signal

As stated in Section 2, most works consider the use of chirp signals for the synchronization signal. For bandwidth B, angular carrier frequency ω_0, and a factor $\beta = \frac{B}{T_s}$, the exponential chirp signal is modeled by

$$s(t) = \psi \text{Re}\left\{e^{j\pi\beta t^k} \cdot e^{j\omega_0 t}\right\}, \quad 0 < t \le T_s \ , \qquad (8)$$

where $\psi = \sqrt{\frac{1}{\frac{T_s}{2}\frac{1}{2}\int_0^{T_s}\cos\left(2\pi\beta t^2\right)dt}} \approx \sqrt{\frac{2}{T_s}}$, and $k \ge 1$. The HFM signal is modeled by

$$s(t) = \sin\left(2\pi b \log(1 + \frac{bt}{P})\right), \quad 0 < t \le T_s \ , \qquad (9)$$

where for frequencies f_1 and f_2, $b = \frac{B}{f_1 f_2 T_s}$ and $P = \frac{1}{f_1}$. Functions $s(t)$ in (8) and (9) are defined as an Up chirp, and $s(T_s - t)$ as a Down chirp.

4. THE UP-DOWN METHOD

Before getting into details, we start by giving an intuition to our method.

4.1 Intuition

Since Doppler shift changes the duration of the received signal by factor $1-\mu$, there is a time difference, denoted by τ_c, between the matching points of an MF for a received

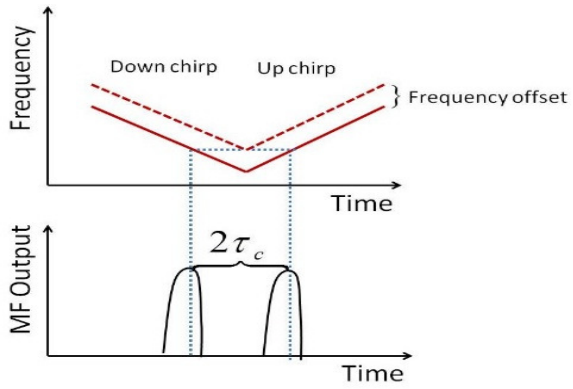

Figure 1: Illustration of Doppler shift effect on Up and Down chirps.

chirp signal with and without Doppler shift. Thus, by finding the relation between τ_c and μ and measuring τ_c, we could estimate μ. Clearly, a direct measurements of τ_c cannot be obtained. Instead, we use a small trick and transmit both Up chirp and Down chirps. In Figure 1, we illustrate the difference between the detected time-of-arrival of both Up and Down chirps for the simplified case of fixed Doppler-induced frequency offset across the symbol bandwidth and no Doppler scaling. The fixed frequency offset in the illustration results a "forward" time shift of τ_c in the matching point of the MF for the Up chirp, and a "backwards" time shift of τ_c in that for the Down chirp. Hence, the time difference between these matching points is $2\tau_c$. Now all is left is to find the relation between τ_c and μ. Unfortunately, different than the analysis of ambiguity functions for radar-based chirp signals [10], in UWAC the time scaling effect of the Doppler shift cannot be neglected and, as we will see, obtaining this relation is not an easy task. Instead, assuming $\beta >> 1$ (see (8)) we approximate the above relation. We note that our method only applies to finding the coarse Doppler shift, and should be followed by a fine tuning for estimating the Doppler shift for the different multipath arrivals.

The advantage of our approach compared to the one presented in [18] (see Section 2) lies in the sampling resolution required for the measured time difference. More specifically, in the latter the measured TDoA is $\frac{T+T_s}{1-\mu}-(T+T_s)$, where T is the time gap between the transmitted pre-ample and post-ample symbols. Thus, the minimum sampling frequency required to separate between two Doppler shift ratios μ_1 and μ_2, where $\mu_1 > \mu_2$, is simply

$$F_{\min}^{\text{Gap-Measure}} = \frac{(1-\mu_1)(1-\mu_2)}{(T+T_s)(\mu_1-\mu_2)} \ . \tag{10}$$

However, we will see that for practical system parameters, the minimum sampling frequency required for our method to differentiate between μ_1 and μ_2 is notably lower. There are two benefits for having a lower minimum sampling frequency. First, it improves complexity. Second, it sets less limitations on the required accuracy level of the TDoA detector (at the output of the MF). The latter is important in UWAC where bandwidth is narrow, and multipath arriving in clusters affect accuracy of the detector. Another advantage of our method is the optional reduction in communication overhead. That is, while the method in [18] requires separate transmission of two chirp signals, we can possibly simultaneously transmit an Up and Down chirps, thus improving throughput.

4.2 Formulating the Matched Filter

While, due to its resilience to Doppler shift, the HFM chirp signal in (9) is also used for sonar detection [7, 15], for simplicity, in this work we focus on the set of exponential chirp signals (8). This is because of the logarithmic operation in (9) which makes it harder to approximate the relation between the Doppler shift ratio and the arrival time. For the same reason, we specifically consider an LFM chirp signal, for which $k = 2$, and a QFM chirp, for which $k = 3$. All forms of chirp signals have similar bandwidth. However, we argue that there is a difference between the resilience of different types of exponential chirp signals (i.e., different k value) to Doppler shift. In fact, while the LFM is more widely used for radar applications (e.g., [17]), we show that the QFM may be a better fit if such resilience to Doppler shift is required. Nevertheless, we provide the mentioned analysis for both LFM and QFM signals.

We start by formulating the MF function for the chirp signal. For the exponential chirp signal in (8), the MF output is

$$\begin{aligned} \text{MF}_k(\tau) &= \int \psi^*(t-\tau)\psi(t)e^{j\omega_0\tau}e^{j\omega_0\mu t} \\ &\cdot \ e^{j\left(\frac{\beta}{k}\right)\left(t^k(1+\mu)^k-(t-\tau)^k\right)}dt \ . \end{aligned} \tag{11}$$

To understand the meaning of τ it is beneficial to simplify (11). Define $\tilde{\psi}_k(t) = \psi(t)e^{j\frac{\beta t^k}{k}}$ and $\omega = \omega_0\mu$. Then, assuming $\int|\tilde{\psi}(t)|^2 = 1$, (11) becomes the ambiguity function

$$\mathcal{X}_k(\tau,\omega) = e^{j\omega_0\tau}\int \tilde{\psi}_k^*(t-\tau)\tilde{\psi}_k(t(1+\mu))e^{j\omega t}dt \ . \tag{12}$$

For $\mu = 0$, $|\mathcal{X}_k(0,0)| = 1$. Then, since τ_c is the time difference between the matching point of the MF with and without Doppler shift, $\tau_c = \underset{\tau}{\text{argmax}}|\mathcal{X}_k(\tau,\omega)|$.

The following correlation envelope and its transformation function will be useful

$$g(t,\tau) = \psi(t-\tau)^*\psi(t) = \int_{-\infty}^{\infty} G(\Omega,\tau)e^{-j\Omega t}\frac{d\Omega}{2\pi} \tag{13a}$$

$$G(\Omega,\tau) = \int_{-\infty}^{\infty} g(t,\tau)e^{j\Omega t}dt \ . \tag{13b}$$

By (11),

$$\begin{aligned} \mathcal{X}_k(\tau,\omega) &= e^{j\omega_0\tau}\int\int dt\frac{d\Omega}{2\pi}G(\Omega,\tau) \\ &\cdot \ e^{-j\Omega t+j\omega t+j\frac{\beta}{k}\left(t^k(1+\mu)^k-(t-\tau)^k\right)} \ , \end{aligned} \tag{14}$$

and for $\psi(t) \approx \sqrt{\frac{2}{T_s}}$, $-\frac{T_s}{2} < t \le \frac{T_s}{2}$ (see (8)) we get

$$G(\Omega,\tau) = e^{\frac{j\Omega\tau}{2}}\frac{2\sin\left[\frac{\Omega T_s}{2}\left(1-\frac{|\tau|}{T_s}\right)\right]}{\Omega T_s} \ . \tag{15}$$

Recall that our objective is to find the relation between τ_c and the Doppler shift ratio, μ. In the following we derive

this relation for two cases: $k = 2$ and $k = 3$, namely the LFM and QFM chirp signals. Since direct maximization of (14) for $k > 1$ is difficult, we approximate $\mathcal{X}_k(\tau, \omega)$.

4.2.1 Solution for LFM

By (14), for $k = 2$ we get

$$\begin{aligned}\mathcal{X}_2(\tau,\omega) &= e^{j\omega_0\tau - j\frac{\beta\tau^2}{2}} \int\int dt \frac{d\Omega}{2\pi} G(\Omega,\tau) \\ &\cdot \quad e^{jt(\omega-\Omega+\beta\tau)+j\beta t^2\mu a_2} , \end{aligned} \tag{16}$$

where $a_2 = \frac{\mu}{2} + 1$. Replacing t with $t + \frac{\tau}{2}$ and defining $\tilde{G}(\Omega,\tau) = \int \psi^*(t - \frac{\tau}{2})\psi(t + \frac{\tau}{2})e^{j\Omega t}dt$, we get

$$\begin{aligned}\mathcal{X}_2(\tau,\omega) &= e^{j\omega_0\tau} \int\int dt \frac{d\Omega}{2\pi} \tilde{G}(\Omega,\tau) \\ &\cdot \quad e^{jt(\omega-\Omega)+j\beta t^2\mu a_2+j\beta t\tau+j\beta t\tau\mu a_2+\phi(\tau)} , \end{aligned} \tag{17}$$

where $\phi(\tau)$ is some function of τ.

Recall $\beta = \frac{B}{T_s}$. In our system we assume $\beta >> 1$. Thus, (17) can be simplified using the saddle point approximation [4]. Define the action value

$$\begin{aligned}\Pi_{k=2}(\Omega,t) &= j(\omega-\Omega)t + j\beta t^2\mu a_2 + j\beta\tau t \\ &+ j\mu a_2\beta\tau t + \phi(\tau) . \end{aligned} \tag{18}$$

The coefficients of the saddle point approximation are

$$\begin{aligned}&\frac{\partial\Pi_{k=2}}{\partial\Omega} = -jt \\ &\frac{\partial\Pi_{k=2}}{\partial t} = j\omega - j\Omega + 2j\mu t\beta a_2 + j\beta\tau(1+a_2\mu) \\ &\frac{\partial\Pi^2_{k=2}}{\partial\Omega^2} = 0, \ \frac{\partial\Pi^2_{k=2}}{\partial t^2} = 2j\mu\beta a_2, \ \frac{\partial^2\Pi_{k=2}}{\partial t\partial\Omega} = -j \\ &\det(\Pi'') = \begin{Vmatrix} 2j\mu\beta a_2 & -j \\ j & 0 \end{Vmatrix} = 1 . \end{aligned} \tag{19}$$

To get a simplification for $\mathcal{X}_2(\tau,\omega)$, define $\Omega_c(\tau) = \omega - \beta\tau(1 + a_2\mu)$ and $t_c = 0$ such that $\Pi(\Omega_c, t_c) = \phi(\tau)$. Then, (16) is approximated by

$$\mathcal{X}_2(\tau,\omega) = e^{j\omega_0\tau - j\phi(\tau)}\tilde{G}(\Omega_c(\tau),\tau) . \tag{20}$$

By (15), the matching point,

$$\underset{\tau}{\text{argmax}}|\mathcal{X}_k(\tau,\omega)| = \underset{\tau}{\text{argmax}}|\tilde{G}(\Omega_c(\tau),\tau) ,$$

is obtained when $\Omega_c(\tau) = 0$ and

$$\tau_c = \frac{\omega_0\mu}{\beta(1+a_2\mu)} = \frac{\omega_0\mu}{\beta(1+\mu+\frac{\mu^2}{2})} . \tag{21}$$

We note that if the Up and Down chirps are not simultaneously transmitted, a compensation factor deducted from τ_c is needed. If the two signals are transmitted one after the other the factor is $\frac{T_s}{1-\mu}$. The expression in (21) is used to estimate μ by measuring the time difference $2\tau_c$.

Let us compare the required minimum sampling resolution in (10) to that required for our method. By (21), for differentiating between Doppler shift ratios μ_1 and μ_2, we require a minimal sampling resolution of

$$F_{\min}^{\text{Up-Down}} = \frac{1}{\tau_c(\mu_1) - \tau_c(\mu_2)} . \tag{22}$$

Consider, $v_1 = 1$ m/sec,$v_2 = 2$ m/sec, $c = 1500$ m/sec, $b = 1000$ Hz, $T_s = 0.01$ sec, $\omega_0 = 40e^3\pi$ rad, and $T = 0.5$ sec, we obtain $F_{\min}^{\text{Up-Down}} \approx 1190$ Hz (i.e., near-Nyquist baseband sampling frequency), while $F_{\min}^{\text{Gap-Measure}} = 2935$ Hz.

4.2.2 Solution for QFM

Following the steps of our saddle point approximation in section 4.2.1, for $k = 3$, we obtain the action value

$$\begin{aligned}\Pi_{k=3}(\Omega,t) &= \frac{j\beta}{3}\left[(t+\tau/2)^3(1+\mu)^3 - (t-\tau/2)^3\right] \\ &- j\Omega t + j\omega t + \phi'(\tau) , \end{aligned} \tag{23}$$

and $\phi'(\tau)$ is some function of τ. Similar to the analysis performed in (19), for $a_3 = 3+3\mu+\mu^2$ we obtain $\Pi_{k=3}(\Omega_c, t_c) = \phi(\tau)$ when $t_c = \frac{T_s}{2}$, and when

$$\Omega_c = \mu\beta a_3 t^2 - \tau\beta(2+\mu\cdot a_3)t + \frac{\beta}{4}\tau^2\mu\cdot a_3 . \tag{24}$$

Then, as in (20), we approximate

$$|\mathcal{X}_3(\tau,\omega)| = \tilde{G}(\mu\beta a_3\frac{T_s^2}{4} - \tau\beta(2+\mu a_3)\frac{T_s}{2} + \frac{\beta}{4}\tau^2\mu a_3,\tau) , \tag{25}$$

which is maximized for $\Omega_c = 0$. Finally, for $k = 3$, we obtain the relation between μ and τ_c,

$$\begin{aligned} 0 &= -\tau_c\beta\left[2+\mu(3+3\mu+\mu^2)\right]\frac{T_s}{2} \\ &+ \mu\beta(3+3\mu+\mu^2)\frac{T_s^2}{4} + \frac{1}{4}\beta\tau_c^2\mu(3+3\mu+\mu^2) \\ &\underset{\mu<<1}{\approx} -\tau_c\beta(2+3\mu)\frac{T_s}{2} + 3\mu\beta\frac{T_s^2}{4} + \frac{3}{4}\beta\tau_c^2\mu . \end{aligned} \tag{26}$$

If deduction of factor $\frac{T_s}{1-\mu}$ from τ_c is needed, (26) becomes a 3rd degree polynomial of μ. We note that the time resolution required in the case of the QFM is similar to that required using the LFM signal.

In the following we use the above analysis to compare the resilience of the LFM and QFM chirp signals to Doppler shift.

4.3 Choosing the Synchronization Signal

Recall the chirp signals we use for estimating the Doppler shift ratio are part of the synchronization signal, which is mainly used for detection of packets and obtaining channel state information. Thus, we are interested in a synchronization signal whose MF output is least affected by Doppler shift. In this section we compare the magnitudes $|\mathcal{X}_2(\tau,\omega)|$ and $|\mathcal{X}_3(\tau,\omega)|$ at the matching point $\tau = 0$. By (15) and (20),

$$|\mathcal{X}_k(0,\omega)| = |\tilde{G}(\Omega_c,0)| = \left|\frac{\sin\left(\frac{\Omega_c T_s}{2}\right)}{\Omega_c T_s/2}\right| . \tag{27}$$

According to Sections 4.2.1 and 4.2.2,

$$\begin{aligned}\Omega_c(\tau=0)|_{k=2} &= \omega_0\mu \\ \Omega_c(\tau=0)|_{k=3} &= \omega_0\mu + \frac{T_s^2}{4}\mu a_3\beta . \end{aligned} \tag{28}$$

The case $\frac{|\mathcal{X}_3(0,\omega)|}{|\mathcal{X}_2(0,\omega)|} > 1$ represents the case where the QFM signal is more resilient to Doppler shift than the LFM signal. From (28), we observe that this is indeed the case.

4.4 Discussion

In Section 4.3 we showed that a QFM chirp signal is expected to have better resilience to Doppler shift than an LFM chirp. In fact, as we will show further below by means of numerical simulations, resilience of a chirp signal to Doppler shift increases with k. However, there are two drawbacks to choosing a higher degree chirp signal. First, the peak-to-average ratio, which is one of the motivations for choosing the chirp signal as the time-synchronization signal, increases with k and affects transmission distortion. Second, for high k value, most of the bandwidth spans over a short fraction of the symbol duration. This means that resilience of the chirp signal to low signal-to-noise-ratio (SNR) decreases as k increases.

5. RESULTS

In this section, we show the performance of our Doppler shift estimation method. The results are presented in terms of the error

$$\rho_e = c|\mu - \hat{\mu}| \,, \tag{29}$$

where $\hat{\mu}$ is the estimated Doppler shift ratio and c is the sound speed. We compare our method (*Up-Down*) to the Doppler estimation method presented in [18] (*Gap-Measure*), as well as to the method described in [11] where Doppler shift is estimated using a bank of matched filters (*MF-Bank*). We avoid comparing our method to estimating the Doppler shift as part of channel parameters or by measuring the Doppler-induced frequency offset (see Section 2). This is because, the former requires a reliable channel model and the later applies to narrowband signals. Clearly, if having small resolution between trial Doppler shift ratios, the MF-Bank method achieves the best performance. However, at cost of complexity that may be too high for real time systems.

In our simulation setting we consider two types of synchronization signals. The first is in the form of an Up chirp followed by a Down chirp and is used for our Up-Down method, as well as for the MF-bank method. The second type of synchronization signal is used by the Gap-Measure method and includes an Up chirp followed by a time gap of $T = 0.5$ sec (used for the information bearing signals) and another Up chirp signal. In both cases, to simulate detection in real scenarios, before and after the synchronization signal we inject a Gaussian noise signal of duration 0.1 sec. For the structure of the chirp signals we use bandwidth of $B = 1000$ Hz, symbol duration $T_s = 0.01$ sec, and angular carrier frequency $\omega_0 = 40e^3\pi$ rad. For comparison, we consider both LFM and QFM chirps.

The simulations include a Monte-Carlo set of 10000 channel realizations. For each simulation, we uniformly generate a Doppler shift ratio, μ, between 0 and 0.003 (which corresponds to a relative speed of up to 4.5 m/sec between the transmitter and receiver for $c = 1500$ m/sec). Given μ, we synthetically interpolate the chirp signals, add an additive Gaussian noise such that the SNR level is 15 dB, and shift it to the baseband frequency while downsampling to rate of $F_{\rm BB}$ Hz. For the Up-Down and Gap-Measured methods we estimate the arrival time by finding the location where the MF output reaches its maximum. For the MF-Bank method, we use a bank of MF with trial Doppler shift resolution which is half of the simulated one. Here, Doppler shift is evaluated by finding the branch number of the MF bank which yields the largest MF output.

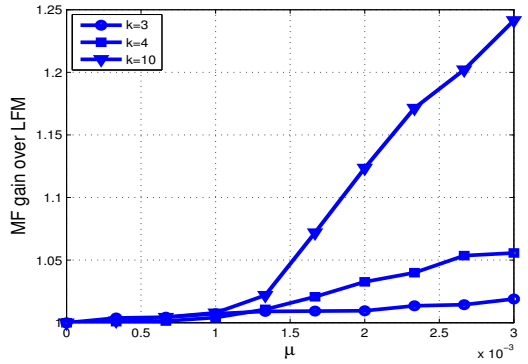

Figure 2: MF gain of chirps over an LFM chirp.

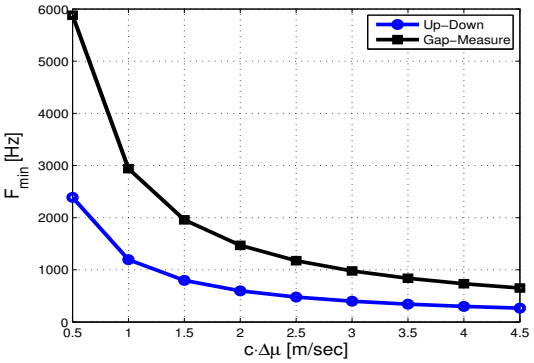

Figure 3: Average results of $F_{\rm min}^{\rm Up-Down}$ from (22) and of $F_{\rm min}^{\rm Gap-Measure}$ from (10) as a function of $\Delta\mu$.

We start by comparing the resilience of chirp signals to Doppler shift. In Figure 2, we show the ratio of the maximum output of the MF for the baseband Doppler-induced chirp signals with $k = 3, 4, 10$ over that of $k = 2$ as a function of μ (recall for LFM $k = 2$ and for QFM $k = 3$). Note that results are averaged over the additive noise. We observe a substantial gain of high order chirp signals over the LFM chirp. We also observe that this gain is not linear. The results show that, on average, resilience to Doppler shift increases with k. However, as noted in Section 4.4, at a cost of resilience to low SNR level and high peak-to-average ratio of the transmitted signals. Since the considered benchmark methods use the LFM chirp signal, in the following we compare estimation results using only an LFM chirp. We note that similar results were obtained using the QFM chirp.

Next, we consider the required sampling resolution to differentiate between two Doppler shift ratios. In Figure 3, we show $F_{\rm min}^{\rm Up-Down}$ from (22) and $F_{\rm min}^{\rm Gap-Measure}$ from (10) as a function of the difference $c\Delta\mu = c(\mu_1 - \mu_2)$. We observe that in all cases $F_{\rm min}^{\rm Up-Down} < F_{\rm min}^{\rm Gap-Measure}$. Hence, using our method, complexity decreases. As we show next, this affects accuracy of the Gap-Measured method at low baseband sampling frequencies.

In Figure 4, we compare the three Doppler shift estimation methods in terms of the error ρ_e from (29). Results

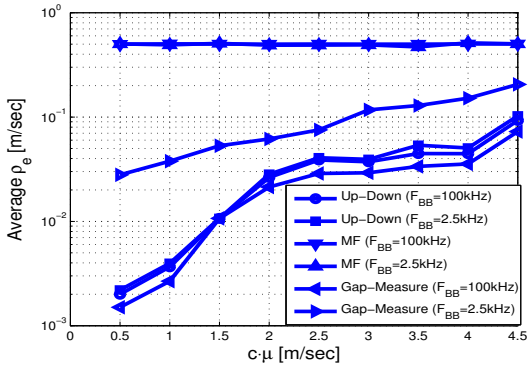

Figure 4: Average ρ_e from (29) for different $F_{\rm BB}$.

are averaged over the random additive noise and are given as a function of μ and the baseband sampling frequency, $F_{\rm BB} > F_{\rm min}^{\rm Up-Down}$. First, we observe that in all methods error increases with μ. This is due to the distortion of the received signals which increases with μ and affects detection accuracy at the output of the MF. Second, comparing accuracy level for different $F_{\rm BB}$ values we observe that, as expected, for the MF-Bank method, accuracy is not affected, while for the Up-Down and Gap-Measure methods, accuracy decreases. However, while in the Gap-Measured method accuracy rapidly decreases with $F_{\rm BB}$, our Up-Down method shows much better resilience to low sampling frequency. From Figure 4, we observe that due to the low resolution of the MF-Bank method, it achieves poor performance. We note that this performance of the MF-Bank method will considerably improve at tested Doppler shift resolution equals that of the simulated one. However, at sometimes significant cost of complexity. For high sampling rate (and thus high complexity) results of the Gap-Measure method exceeds that of our Up-Down method. This is because of the saddle point approximation done in (20). However, at near-Nyquist baseband sampling rate, significant improvement is shown using our method.

6. CONCLUSIONS

In this paper, we presented a method to estimate the coarse Doppler shift for UWAC. Our method is based on the relation between the Doppler shift ratio and the Doppler-induced time shift at the arrival time of the received signal. Based on transmitting an "Up" and "Down" chirp signals, we presented a way to calculate this time shift, and developed an approximations for the above relation for UWAC, where Doppler shift affect on symbol duration is non-negligible. We derived a solution for both LFM and QFM chirp signals. This analysis provided an interesting insight showing that the QFM chirp is more resilient to Doppler shift than the LFM chirp, which is widely used for radar applications. Simulation results demonstrated the advantage of our method over benchmark Doppler estimation methods. Further work would include a similar analysis for HFM chirp signal, and an optimization of the structure of the synchronization signal in terms of resilience to Doppler shift.

7. REFERENCES

[1] I. F. Akyildiz, D. Pompili, and T. Melodia. On the relationship between cpacity and distance in an underwater acoustic communication channel. In *ACM International Workshop on UnderWater Networks (WUWNet)*, Sep. 2006.

[2] I. F. Akyildiz, D. Pompili, and T. Melodia. State of the art in protocol research for underwater acoustic sensor networks. In *ACM International Workshop on UnderWater Networks (WUWNet)*, Sep. 2006.

[3] W. Burdic. *Underwater Acoustic System Analysis*. Peninsula Publishing, Los Altos, USA, 2002.

[4] R. W. Butler. *Saddlepoint Approximations with Applications*. Cambridge University Press, Cambridge, United Kindom, 2007.

[5] M. Chitre, S. Shahabudeen, and M. Stojanovic. Underwater acoustic communications and networking: Recent advances and future challenges. *Marine Technology Society*, 42(1):103–116, Apr. 2008.

[6] A. Fish, A. Sayeed, S. Gurevich, R.Hadani, and O. Schwartz. Delay-doppler channel estimation with almost linear complexity. In *IEEE International Symposium on Information Theory Proceedings (ISIT)*, pages 2386–2390, jul. 2012.

[7] R. Gieleghem. *Robust acoustic signal detection and synchronization in a time varying ocean environment*. Master Thesis, Woods Hole Oceanographic Institution, Sep. 2012.

[8] N. Josso, J. Zhang, D. Fertonani, A. Papandreou-Suppappolat, and T. Duman. Time-varying wideband underwater acoustic channel estimation for OFDM communications. In *IEEE Conference on Acoustics Speech and Signal Processing (ICASSP)*, pages 5626–5629, Mar. 2010.

[9] N. Josso, J. Zhang, A. Papandreou-Suppappolat, C. Ioana, J. Mars, C. Gervaise, and Y. Stephan. Doppler estimation and correction for shallow underwater acoustic communications. In *IEEE OCEANS Conference*, pages 1–6, Oct. 2009.

[10] N. Levanon. *Radar Principles*. John Wiley and Sons, 1988.

[11] M. Palmese, G. Bertolotto, A. Pesceto, and A. Trucco. Experamental validation of a chirp-based underwater acoustic communication method. In *International Acoustic Conference*, pages 440–445, Jul. 2008.

[12] K. Perrine, K. Nieman, T. Henderson, K. Lent, T. Brudner, and B. Evans. Doppler estimation and correction for shallow underwater acoustic communications. In *International Conference on Signals, Systems and Computers (ASILOMAR)*, pages 746–750, Nov. 2010.

[13] R. Peterson, R. E. Ziemer, and D. E. Borth. *Introduction to Spread Spectrum Communication*. Prentice-Hall, 1995.

[14] O. Rabaste and T. Chonavel. Estimation of multipath channels with long impulse response at low SNR via an MCMC method. *IEEE Transactions on Signal Processing*, 55(4):1312–1325, Apr. 2007.

[15] X. Song, P. Willett, , and S. Zhou. Range bias modeling for hyperbolic frequency modulated waveforms in target tracking. *IEEE Journal of Oceanic Engineering*, 2012. To Appear.

[16] L. Wan, Z. Wang, S. Zhou, T. C. Yang, and Z. Shi.

Performance comparison of doppler scale estimation methods for underwater acoustic OFDM. *Hindawi Journal of Electrical and Computer Engineering*, 2012, Apr. 2012.

[17] B. Wang, G. Yang, and G. Liu. A noval join estimation algorithm for multi-parameter of underwater acoustic channels. *Journal of Information Technology*, 10(2):440–445, 2011.

[18] L. Wu, J. Trezzo, D. Mirza, P. Roberts, J. Jaffe, Y. Wang, and R. Kastner. Designing an adaptive acoustic modem for underwater sensor networks. *IEEE Embedded Systems Letters*, 4(1):1–4, Mar. 2012.